Axonal TAU sorting in SH-SY5Y-derived neurons requires the C-terminus of TAU but is independent of Ankyrin G

Bell, M.[1,2], Bachmann, S.[1,2], Klimek, J.[1,2], Langerscheidt, F.[1,2,3], Zempel, H.[1,2]

[1] Institute of Human Genetics, University Hospital Cologne, Kerpener Str. 34, 50931 Cologne, Germany.

[2] Center for Molecular Medicine Cologne (CMMC), Robert-Koch-Str. 21, 50931 Cologne, Germany.

[3] FB03 Chemistry and Biotechnology, Campus Jülich, Fachhochschule Aachen, Heinrich-Mußmann-Straße 1, 52428 Jülich, Germany.

Correspondence:

Michael Bell, Center of Molecular Medicine Cologne (CMMC), Robert-Koch-Str. 21, 50931 Cologne, michael.bell@uk-koeln.de.

Hans Zempel, Institute of Human Genetics, University Hospital Cologne, Kerpener Str. 34, 50931 Cologne, Germany, hans.zempel@uk-koeln.de

Abstract

Somatodendritic missorting of the axonal protein TAU is a hallmark of Alzheimer's disease and related tauopathies. Cultured rodent primary neurons and iPSC-derived neurons are often used for studying mechanisms of neuronal polarity, including TAU trafficking. However, these models are expensive, time-consuming and/or require the sacrification of animals. In this study, we show that neurons derived from SH-SY5Y neuroblastoma cells, generated with a RA/BDNF-based differentiation procedure, are suitable for investigating axonal TAU sorting. These SH-SY5Y-derived neurons show pronounced neuronal polarity, axodendritic outgrowth, expression of the neuronal maturation markers TAU and MAP2, and, importantly, efficient axonal sorting of endogenous and transfected human wild type TAU. By using SH-SY5Y-derived neurons and mouse primary neurons, we demonstrate that axonal TAU enrichment requires the presence of the TAU C-terminal half, as a truncated C-terminus-lacking construct (N-term-TAU^{HA}) is localized in the soma, where it accumulates. Moreover, SH-SY5Y-derived neurons do not show classical axon initial segment (AIS) formation, indicated by the lack of Ankyrin G (ANKG) enrichment at the proximal axon, which suggests that successful axonal TAU sorting is independent of complete AIS formation. Taken together, our results suggest i) that SH-SY5Y-derived neurons are a valuable human neuronal model for studying TAU sorting, which is readily accessible at low cost and without animal need, and that ii) the mechanisms of axonal TAU targeting require the TAU C-terminal half but no ANKG enrichment at the proximal axon.

Key words: TAU sorting, Alzheimer's disease, SH-SY5Y-derived neurons, Neuronal polarity, Ankyrin G

Introduction

The microtubule-associated protein TAU is highly abundant in the axons of healthy brain neurons [1,2], where six isoforms are predominantly expressed [3,4]. By binding microtubule (MT) filaments, TAU regulates their assembly and disassembly [5–7], and is thereby involved in axonal outgrowth, plasticity, MT-dependent cargo transport and other cellular functions [8–12]. The C-terminal repeat domains and their flanking regions bind the MTs [13,14], while the N-terminus acts as a spacer between adjacent MT filaments and mediates membrane interactions [15–17]. Missorting of highly phosphorylated TAU into the somatodendritic compartment and the formation of insoluble TAU aggregates ('neurofibrillary tangles') are major hallmarks of Alzheimer's disease (AD) and related tauopathies [18–23]. Subcellular TAU mislocalization leads to a lack of axonal TAU-MT interaction, a depletion of stable MT filaments and, eventually, to disruption of axonal transport [24–26]. In the dendrites, abnormal amounts of hyperphosphorylated TAU trigger TTLL6-mediated MT destabilization and spine loss, FYN-mediated excitotoxicity, and other processes that lead to postsynaptic degradation [27–32].

Understanding the mechanisms of axonal TAU sorting in healthy neurons is a critical step towards the elucidation of pathological processes that accompany TAU missorting. Several mechanisms are thought to drive axonal TAU sorting (reviewed in [33,34]), including active anterograde TAU trafficking, selective axonal TAU-MT interactions, or active retrograde retention of axonal TAU. In this context, the axon initial segment (AIS), a key player for developing and maintaining neuronal polarity with Ankyrin G (ANKG) as a master organizer of the molecular structure (reviewed in [35–37]), may be relevant, as polarized MT filaments within the AIS are involved in motor protein-mediated soma-to-axon-trafficking (reviewed in [35,38]), presumably including TAU transit [33,34]. Moreover, recent studies found direct evidence for a retrograde TAU diffusion barrier within the AIS that is compromised by MT disassembly [39,40]. Notably, little is yet known about the intrinsic components of TAU, i.e. functional domains, interaction motifs, post-translational modifications and relevant TAU interactions, although some recent studies in rodent primary neurons assumed major roles for phosphorylation sites within the Proline-rich region and for the very N-terminal domain of TAU but a minor role for the four MT-binding repeat domains [41,42].

Which neuronal cell models are available to address these key aspects of TAU sorting and missorting? Two commonly used cellular systems are rodent primary neuron cultures [39–42] and recently also human induced pluripotent stem cell (iPSC)-derived neurons [43–47]. Both systems have considerable limitations. Rodent primary neuronal cultures require the use and sacrification of animals, and rodent Tau differs in several aspects from human TAU, e.g. regarding the isoform expression pattern [48]. In addition, the human cellular environment, i.e. the entire sorting machinery and interaction partners may differ from that in humans. Overexpressed human TAU often appears uniformly distributed in rodent primary neurons [49]. IPSC-derived neurons overcome many of these issues, but their generation is expensive, time-consuming and results in mixed cultures with variable homogeneity and differentiation efficiency [50–52]. The neuroblastoma cell line SH-SY5Y is human-derived [53] and cell can be differentiated with various

substances into polarized neuronal cells (SH-SY5Y-derived neurons) at low cost (reviewed in [54]). SH-SY5Y-derived neurons express common neuronal maturation marker proteins [55–60], including all six major human TAU isoforms [61,62], show proper axonal TAU localization, and mimic the phosphorylation state of TAU in the adult human brain [63–66]. In brief, SH-SY5Y-derived neurons unite the benefits of a cell line, i.e. robust maintenance, fast growth rates, the saving of animal resources and simple accessibility for stable genetic engineering [67,68], with polarized and mature neuronal cultures.

In this study, we evaluated four differentiation procedures of SH-SY5Y cells for generating neuronal cells and tested their suitability for the investigation of TAU sorting. We show that RA/BDNF-treated SH-SY5Y-derived neurons achieve cellular polarity, axonal outgrowth, strong upregulation of the neuronal markers TAU and MT-associated protein 2 (MAP2), and, importantly, efficient axonal sorting of endogenous TAU, and also of overexpressed and HA-tagged TAU (0N3R-TAU^{HA}). In contrast, TAU lacking the C-terminal half (N-term-TAU^{HA}) was retained in the soma of SH-SY5Y-derived and mouse primary neurons. Of note, SH-SY5Y-derived neurons do not show ANKG enrichment at the proximal axon despite successful axonal TAU targeting, suggesting an ANKG-independent mechanism of axonal TAU enrichment. In brief, our results give evidence that i) SH-SY5Y-derived neurons show successful axonal sorting of endogenous and transfected human TAU, ii) the N-terminus of TAU is not sufficient for proper axonal sorting, and ii) the axonal targeting of endogenous and 0N3R-TAU^{HA} is independent of ANKG, a master organizer of the AIS molecular structure.

Methods

Molecular biology

For experiments with endogenous and recombinant TAU, an expression vector, which harbored the cDNA encoding for tdTomato, was used as volume marker control.

For experiments with recombinant TAU constructs, N-terminally tagged 0N3R-TAU^{HA} and N-term-TAU^{HA} constructs were cloned into the same, CMV promoter-containing expression vector (see Suppl. Sequence 1 for sequence of 0N3R-TAU^{HA} vector). For this, the intended TAU cDNA sequences were amplified by PCR using primer pairs with restriction sites (AgeI, BamHI) corresponding to the multiple cloning site of the backbone vector. Additionally, the forward primer contained an HA tag sequence overhang with start codon (5'-ATGTACCCATACGATGTTCCAGATTACGCT-3'), which was hence fused to the 5' site of the TAU sequence. The PCR product was analyzed via gel electrophoresis, and correctly sized inserts were cut out and purified with NucleoSpin™ Gel & PCR Clean up Kit (Macherey & Nagel). Vector and insert were digested (30 min, 37 °C) according to manufacturer's protocols (enzymes by New England Biolabs), either purified directly (insert) or from agarose gel (vector) and ligated (16 – 18 h, 20 – 22 °C) with T4 DNA ligase (NEB) according to the manufacturer's protocol.

For plasmid amplification, plasmids were transformed into chemocompetent bacteria (*E. coli* Top10™, Thermo Fisher Scientific, TFS), that were generated like previously described (Sambrook and Russell, 2006). Bacteria were spread onto pre-warmed agar plates with antibiotics (16 – 18 h, 37 °C), colonies were picked and grown in nutrient medium with antibiotics. For plasmid isolation and purification from bacterial suspensions, the PureYield™ MidiPrep Kit (ProMega) or NucleoBond Xtra™ Midi/Maxi Kit (Macherey & Nagel) were used according to the manufacturer's protocols. Plasmid concentration and purity were checked spectrophotometrically (NanoDrop™ 100, TFS) and isolates were long-term stored at -20 °C.

SH-SY5Y cell cultivation and differentiation

Maintenance. The SH-SY5Y neuroblastoma cell line was kindly provided by Prof. Dr. Rudolf Wiesner (Institute of Veg. Physiology II, University Hospital Cologne). SH-SY5Y cells were cultured in DMEM/F12 (#10565-018, TFS) supplemented with 10 % fetal bovine serum (FBS, Biochrom AG), penicillin/streptomycin and amphotericin B (1X Anti/Anti, #15240062, TFS) (referred to as 'SHM-10') on uncoated cell culture flasks (VWR). Cultures were maintained in a sterile incubator (MCO-20AIC, PHCbi) at 37 °C, 95 % air humidity and 5 % CO_2 concentration. Culture medium was changed once or twice per week, depending on cell density, and cells were passaged for further cultivation or differentiation experiments at 70 – 80 % confluency. For passaging, SH-SY5Y cells were washed with DPBS, trypsinized (0.05 % Trypsin/EDTA, TFS) for 3 – 5 minutes, spun down at 1000 g for 3 minutes and resuspended in SHM-10. For differentiation experiments, resuspended SH-SY5Y cells were counted with automatic cell counter (TC20™, Bio-Rad) and seeded with 7.5 to 10 x 10^3 cells per cm² on glass coverslips (VWR), coated with 20 µg/ml Poly-D-lysine (PDL, AppliChem) for at least 3 h at 37 °C. For long-term storage, trypsinized and spun down cells were resuspended in FBS with 10 % DMSO, cooled down with -1 °C / min in a cryo container (Mr. Frosty™, VWR) and stored at -80 °C or in liquid nitrogen.

Differentiation. Differentiation protocols were started 24 h after seeding. For RA-based differentiation, fresh SMM with 10 µM retinoic acid (RA, Sigma-Aldrich) was added at day 0 (d0) and replaced every 2 – 3 days up to d7. Differentiation with RA & brain-derived neurotrophic factor (BDNF, Peprotech) was adapted from [55]. Briefly, after RA treatment up to d7 as described above, cells were washed once with DPBS, and SHM-10 medium without FBS (referred to as 'SHM-0') containing 10 ng/ml BDNF was added and once replaced until d14. Differentiation protocols for Phorbol-12-myristate-13-acetate (TPA)- and RA/TPA-based differentiation were adapted from [59,69]. In brief, fresh SHM-10 with 81 µM TPA (Sigma-Aldrich) was added and replaced every 2 – 3 days until d9 for TPA-based differentiation. For RA & TPA-treatment, fresh SHM-10 with 10 µM RA was added, replaced after 2 – 3 days up to d4 or d5, whereupon

cells were washed once with PBS and cultivated in fresh SHM-10 with 81 µM TPA until d9 with one medium change in between.

Two alternative long-term differentiation procedures were tested for RA, RA/TPA and TPA treatments. The first variant (variant A) included cultivation with RA (for RA & RA/TPA protocols) and TPA (TPA protocol) in SHM-10 until d7, cultivation with RA (RA protocol) and TPA (RA/TPA & TPA protocols) in SHM-10 with 3 % FBS (SHM-3) until d9, and cultivation with RA (RA protocol) and TPA (RA/TPA & TPA protocols) in SHM-0 until d14. The second variant (variant B), where the seeding density was increased (15 to 20 x 10^3 cells per cm^2), included cultivation with RA (for RA & RA/TPA protocols) and TPA (TPA protocol) in SHM-10 until d2, cultivation with RA (RA & RA/TPA protocols) and TPA (TPA protocol) in SHM-3 until d7, cultivation with RA (RA protocol) and TPA (RA/TPA & TPA protocols) in SHM-3 until d9, and cultivation with RA (RA protocol) and TPA (RA/TPA & TPA protocols) in SHM-0 until d14 (see Suppl.Fig. 1).

Transfection

SH-SY5Y-derived neurons were transfected using the polymer-based PolyJet™ DNA transfection reagent (#SL100688, SignaGen) between d2 and d5 of differentiation. Transfection was performed according to the manufacturer's protocol with the following modifications: Before transfection, conditioned medium was collected from each well and stored at 37 °C with 5 % CO_2. For one well of a 24-well plate, 0.33 µg (6-well: 0.66 µg) of plasmid DNA and 1.0 µl (6-well: 2.0 µl) PolyJet™ reagent were separately prepared with 25 µl (6-well: 50 µl) DMEM (#P04-03500, TFS), then mixed, incubated and added dropwise to the cultures. Medium was changed to previously collected, conditioned medium, supplemented with fresh doses of RA or TPA, 3 – 16 h after transfection. Transfection efficiency ranged from 5 – 10 %. For experiments with recombinant TAU, tdTomato- and TAU^{HA} construct-encoding plasmids were co-transfected in SH-SY5Y-derived neurons. For this, DNA of both plasmids was incubated commonly with PolyJet™. The plasmid DNA was mixed with a ratio of three (TAU^{HA} plasmid) to one part (tdTomato plasmid). The total DNA amount per well was not altered, i.e. 0.33 µg was used per one well of a 24-well plate.

Primary neurons cultivation

Isolation. Pregnant female FVB wild type mice were anesthetized and sacrificed at day 13.5 of pregnancy by authorized personal with respect to the official regularities and guidelines of the government authority, the Landesumweltamt (LANUV) of North Rhine-Westphalia, Germany. Preparation of E13.5 embryos, and isolation and cultivation of primary neurons were performed like previously described [70]. In brief, embryos were decapitated, embryonic scalp, skull and meninges were removed, the cerebral hemispheres were isolated, washed, dissociated for 5 – 7 minutes with 0.05 % Trypsin/EDTA (TFS), and homogenized in HBSS (w/o Ca^{2+}/Mg^{2+}, #14185052, TFS). Dissociated primary cells were counted as described above for SH-SY5Y cells and seeded with 5 to 7.5 x 10^4 cells per cm^2 in neuronal plating medium (NPM), i.e. Neurobasal™ medium (#21103, TFS) supplemented with 1 % FBS, penicillin/streptomycin and amphotericin B (1X Anti/Anti), GlutaMAX™ (1X, TFS) and NS-21 (1X, #P07-20001, PAN Biotech), on glass coverslips (VWR), coated with 20 µg/ml Poly-D-lysine (PDL, AppliChem) for at least 3 h at 37 °C.

Maintenance. Four days after seeding, the medium was doubled by adding neuronal maintenance medium (NMM), i.e. NPM without FBS. Cytosine arabinoside (Ara-C, #C1768, Sigma-Aldrich) was added to an end concentration of 0.5 – 1.0 µg/ml to impair survival of proliferating glial, endothelial and other cells.

Transfection. Mouse primary neurons were transfected at day 6 in vitro (div6). Transfection was performed as described elsewhere [71].

In brief, 0.25 µg of plasmid DNA and 0.375 µl Lipofectamine ™ 2000 (#743517, Invitrogen) were mixed for one well of a 24-well plate, incubated for 30 minutes and added dropwise to the cultures. Medium was changed to previously collected, conditioned medium 60 minutes after transfection. For experiments with recombinant TAU, tdTomato- and TAU^{HA} construct-encoding plasmids were co-transfected in mouse primary neurons. For this, the DNA of both plasmids was mixed with a ratio of three parts (TAU^{HA}

DNA) to one part (tdTomato DNA) before addition of Lipofectamine™ 2000. The total DNA amount per well was not altered, i.e. 0.25 µg per 24-well (1 µg per 6-well) was used.

Fixation & Immunofluorescence

Fixation and immunofluorescence of cell cultures was done as previously described [70] with slight modifications. In brief, cells were fixed for 1 h (for experiments on ANKG expression: 1 h or 30 min) with 3.7 % formaldehyde (in PBS), permeabilized and blocked with 5 % bovine serum albumin (BSA, Sigma-Aldrich) and 0.1 % Triton X-100 (AppliChem) in PBS for 5 minutes, incubated with the primary antibody (diluted in PBS) either for 2 – 3 h at 20 – 22 °C or at 4 °C overnight, incubated with the corresponding secondary antibody (diluted in PBS), coupled to AlexaFluor™ fluorophores, for 1 – 2 h at 20 – 22 °C. The following primary antibodies were used: rabbit anti-TAU (K9JA) (1:1000, #A0024, DAKO), rabbit anti-HA (1:1000, #3724S, cellSignaling), mouse anti-HA (1:1000, #901533, BioLegend), chicken anti-MAP2 (1:2000, ab5392, Abcam), mouse anti-ANKG (N106/36) (1:250, MABN466, Neuromab). Nuclei were stained with NucBlue™ (1 drop/ml, TFS) for 20 – 30 minutes, and samples were mounted on objective slides (#145-0011, Bio-Rad) using PolyMount™ (#18606, Polysciences) or Mowiol™ (AppliChem) mounting medium, dried for 24 h at RT and long-term stored at 4 °C in the dark.

Microscopy

Immunostained cells were imaged with a wide field fluorescence microscope (Axioscope 5, Zeiss), using an LED excitation lamp (Colibri 7, Zeiss), a fluorescence camera device (Axiocam 503 mono, Zeiss), objectives with 10 x, 20 x, 40 x (air-based) and 63 x (oil-based) magnification (Zeiss) and Zen imaging software (Zen Blue pro, Zeiss). Exposure time and light intensity were adjusted to avoid excessive sample bleaching and to preclude saturation of fluorescent signal detection. For the analysis of protein expression levels, all images were taken with identical settings regarding laser intensity and exposure time to ensure statistical comparability. For documentation during cell cultivation, images were taken with a brightfield light microscope (DM IL LED, Leica) using objectives with 10x and 20 x (air-based) magnification (Leica) and Las X imaging software (Leica).

Data analysis

Differentiation Efficiency. The efficiency of SH-SY5Y cell differentiation was defined as relative number of SH-SY5Y-derived neurons compared to undifferentiated cells. SH-SY5Y cells were considered as differentiated if they fulfilled the following morphological criteria: i) roundish shaped soma, ii) changed nuclear morphology, i.e. smaller and brighter nuclear signal, iii) axonal outgrowth exceeds soma diameter at least twofold and iv) determined axon length exceeds 50 µm. Further analysis was performed only with cells reaching these criteria.

Axonal outgrowth. Axonal outgrowth of SH-SY5Y-derived neurons was determined using Fiji/ImageJ software (NIH). The processes were traced manually, and axon length was determined as pixel number, transformed to absolute distances with respect to the original image resolution. The measured section reached from the soma-to-axon-border to the most distal axonal part, which was still detectable. Included cells fulfilled the described differentiation criteria and the axon was distinctive from processes of adjacent cells.

Endogenous protein expression. For the analysis of total endogenous expression of the neuronal maturation markers TAU and MAP2, SH-SY5Y-derived neurons were analyzed with Fiji/ImageJ software. Entire cells were encircled manually, and the mean fluorescence intensity (MFI_{neuron}) of this marked region of interest (ROI) was determined. To exclude background noise, MFI of an empty area next to the neuron was determined in the same manner (MFI_{noise}) and subtracted from the MFI_{neuron}. Further, MFI was determined in absence of primary antibodies ($MFI_{unspecific}$), and also subtracted from MFI_{neuron} to eliminate impact of unspecific binding of the secondary antibody. Protein levels of differentiated cells were normalized to that of undifferentiated cells. To ensure comparability of protein levels, all cell cultures of one experiment were cultivated on the same plate, immunostained and mounted in parallel with identical antibody solutions and imaged with identical microscope settings.

Axonal enrichment of endogenous TAU. By using Fiji/ImageJ, one region within the soma, which had no overlap with the Hoechst signal, was set as first ROI for each analyzed SH-SY5Y-derived neuron. An axonal segment of around 5 – 10 µm in 50 – 75 µm distance to the soma was chosen as second ROI. TAU signals were measured as MFI for both somatic and axonal ROIs (MFI_{soma}, MFI_{axon}). To exclude background noise, MFI of empty areas next to the soma and axon were determined in the same manner ($MFI_{noiseSoma}$, $MFI_{noiseAxon}$) and subtracted from the MFI_{soma}/MFI_{axon}. The ratio of MFI_{axon} and MFI_{soma} was calculated (axon-to-soma-ratio). The axon-to-soma-ratio of the volume marker tdTomato was determined using identical ROIs and identical calculation steps. The axon-to-soma-ratio of TAU was normalized to this of tdTomato to achieve the axonal enrichment factor of TAU (AEF_{TAU}). Only tdTomato-positive SH-SY5Y-derived neurons were included for analysis.

Axonal enrichment of TAU^{HA} constructs. ROI selection and calculation of the axonal enrichment factor of TAU^{HA} constructs (AEF_{TAU_HA}) were done as described above for endogenous TAU with a few deviations. Instead of TAU signals, the intensity of anti-HA signal was measured. Only cells that were successfully co-transfected with tdTomato and TAU^{HA} were included for analysis. Further, to overcome signal of unspecific anti-HA antibody binding, HA tag MFIs of somatic and axonal ROIs from untransfected cells ($MFI_{unspecificSoma}$, $MFI_{unspecificAxon}$) were measured and averaged for each experiment and subtracted from all MFIs of TAU^{HA} from transfected cells.

AIS expression profile. The expression profiles of ANKG and NRCAM signals were determined at the proximal axon of SH-SY5Y-derived and mouse primary neurons by using Fiji/ImageJ software. The first 75 µm of the axon, starting with the soma-to-axon border, of neurons were traced with a segmented line (thickness: three pixels), and a plot profile was created. To exclude influence of crossing neurites and unspecific background, a plot profile of the region right next to the axon was measured and subtracted from the original value. Further, a plot profile was determined in absence of primary antibodies and subtracted from the sample values to eliminate impact of unspecific binding of the secondary antibody.

Statistical analysis. All statistical calculations were performed using PRISM™ (V8.3, GraphPad) analysis software. For comparisons between one group of samples and a constant number (e.g. 1.0) or between two groups of samples, a two-sided student's t-test was used for the determination of p-values. When multiple groups were tested for significant differences, a Brown-Forsythe-test was applied to check if the standard deviation (SD) differed significantly ($p \geq 0.05$) among the tested groups. If this was the case, a Brown-Forsythe and Welch ANOVA test with Dunnett's T3 correction for multiple comparisons was conducted. If SD was not significantly different ($p < 0.05$), an ordinary one-way ANOVA test with Tukey's correction for multiple comparisons was conducted. The chosen statistical tests are mentioned for all experiments in the corresponding figure legends. Significance levels are symbolized with asterisks if $p < 0.05$ (*), $p < 0.01$ (**) or $p < 0.001$ (***).

Results

RA/BDNF treatment produces homogeneous cultures of highly polarized neurons

We first aimed to investigate whether SH-SY5Y-derived neurons are suitable for studying TAU sorting. For this, naïve human SH-SY5Y neuroblastoma cells (Fig. 1A) were differentiated using four distinct procedures (Fig. 1B). Cells were either treated only with retinoic acid (RA) until day 7 of differentiation (d7), with RA until d7 followed by brain-derived neurotrophic factor (BDNF) in serum-free conditions until d14, with the phorbol ester TPA until d9 or with RA until d4 followed by TPA until d9. To compare the amount of successfully differentiated neurons, cells were classified as differentiated when they fulfilled several differentiation criteria, e.g. roundish shaped somata and axonal processes of at least 50 µm length (see methods for details). While treatment with RA (52.5 % ± 11.8 % neurons), TPA (39.7 % ± 10.2 %), and RA/TPA (47.4 % ± 5.4 %) generated mixed cultures of undifferentiated and neuronal cells, the sequential RA/BDNF treatment resulted in high numbers of SH-SY5Y-derived neurons (74.1 % ± 11.4 %) (Fig. 1C,D).

RA/BDNF-treated SH-SY5Y-derived neurons show pronounced axonal outgrowth and high levels of neuronal maturation markers

Next, the neuronal maturity of SH-SY5Y-derived neurons upon the four treatments was evaluated both morphologically and biochemically. The axonal outgrowth of SH-SY5Y-derived neurons was determined as the distance from the soma-to-axon-border to the distal axonal end. The average axonal outgrowth in RA/BDNF-induced neurons (264 µm ± 43 µm) exceeded the axon length of all other cultures significantly, namely RA (141 µm ± 21 µm), RA/TPA (125 µm ± 28 µm), and TPA (76 µm ± 10 µm), indicating the highest level of neuronal polarity in RA/BDNF-induced SH-SY5Y-derived neurons (Fig. 2A,C). Next, we tested the expression of two commonly used marker proteins for neuronal maturation [72], TAU and the somatodendritically localized MT-associated protein 2 (MAP2) in SH-SY5Y-derived neurons (Fig. 2B). The expression of TAU was upregulated 12-fold (± 4.6) in RA/BDNF-treated neurons compared to undifferentiated SH-SY5Y cells. A similar increase of TAU protein levels was observed upon RA/TPA treatment (9.6-fold ± 2.8). Treatment only with RA (6.4-fold ± 3.3) or TPA (5.6-fold ± 2.6) led to less strong increases of TAU levels (Fig. 2D). MAP2 levels were strongly elevated in neurons after RA/BDNF treatment (8.8-fold ± 3.6), with notable inter-experimental variability. The MAP2 levels were moderate after differentiation with RA (3.7-fold ± 1.6), RA/TPA (4.1-fold ± 2.2), and no significant difference was observed between TPA (1.8-fold ± 1.1) and undifferentiated SH-SY5Y cells (Fig. 2E).

Attempts of cultivating SH-SY5Y cells in RA, TPA or RA/TPA under serum-reduced conditions were not successful, i.e. cultures largely died after the transfection procedure (Suppl.Fig. 1C-H), in contrast to transfected RA/BDNF-treated cultures (Suppl.Fig. 1A,B).

Taken together, RA/BDNF-treated SH-SY5Y-derived neurons showed the highest differentiation efficiency, pronounced neuronal maturation, indicated by the pronounced axonal outgrowth and the highest expression levels of TAU and MAP2, and also tolerated protein overexpression for at least nine days upon transfection.

Endogenous TAU is efficiently sorted in SH-SY5Y-derived neurons upon RA/BDNF treatment

To further evaluate the suitability of SH-SY5Y-derived neurons for TAU sorting studies, the efficiency of endogenous TAU neurons was determined. For this, the cells were transfected with tdTomato-expressing plasmids at d5 as described (see methods for details), and the axonal enrichment factor of TAU ($AEF_{endoTAU}$) was defined as axon-to-soma-ratio of TAU normalized to the axon-to-soma-ratio of randomly unbiased distributing tdTomato (see methods for details).

Mainly axonal TAU signal and strong somatic tdTomato signals indicate a strong and efficient axonal sorting of TAU in RA/BDNF-treated neurons ($AEF_{endoTAU}$ = 7.9 ± 1.2), but less efficient axonal sorting in RA- (2.6 ± 0.9), RA/TPA- (3.3 ± 0.6) and TPA-treated neurons (3.4 ± 0.8) (Fig. 3A,B). Except for RA-induced neurons (p = 0.07, n.s.) the $AEF_{endoTAU}$ of all differentiated cells was significantly higher than 1.0, namely for RA/BDNF- (p = 0.0002, ***), RA/TPA- (p = 0.02, *), and TPA-treated neurons (p = 0.009, **), indicating differently efficient axonal TAU enrichment in these cells. In brief, these $AEF_{endoTAU}$ values suggests efficient axonal TAU sorting in RA/BDNF-treated SH-SY5Y-derived neurons, comparable to cultured primary mouse forebrain neurons (Fig. 4D, Suppl.Fig. 2), an often-used neuronal cell model for TAU sorting. Since the results of the comparative analyses revealed RA/BDNF-treated SH-SY5Y-derived neurons as the most suitable system in many respects, i.e. we observed efficient differentiation procedure, pronounced neuronal polarity, efficient sorting of endogenous TAU, and unchanged viability up to nine days after transfection, only those neurons were used for all further experiments.

RA/BDNF-treated SH-SY5Y-derived neurons show robust sorting of overexpressed 0N3R-TAU^{HA}

Efficient axonal sorting of transfected and overexpressed TAU constructs is an often-faced problem in primary neuron models [49]. Therefore, we checked whether SH-SY5Y-derived neurons achieve endogenous-like sorting of transfected and overexpressed human wild type TAU. For this, we co-transfected SH-SY5Y-derived neurons with tdTomato and the shortest TAU isoform, bound to an N-terminal HA tag (0N3R-TAU^{HA}), which was under CMV promoter control, at d5 of differentiation. Strikingly, the axonal enrichment of the overexpressed 0N3R-TAU^{HA} (AEF_{TAU_HA} = 7.4 ± 1.3; ~ 94 % of $AEF_{endoTAU}$) was significantly higher than 1.0 (p = 0.01, *) and similar to axonal targeting of endogenous TAU in RA/BDNF-treated SH-SY5Y-derived neurons at d14 (Fig. 4A,C). In mouse primary neurons, 0N3R-TAU^{HA} was axonally sorted (t-test for difference from 1.0: p = 0.02, *), but less efficient than endogenous Tau (AEF_{TAU_HA} = 5.8 ± 2.1, ~ 45 % of $AEF_{endoTau}$) (Fig. 4D, Suppl.Fig. 2). These results highlight the ability of

SH-SY5Y-derived neurons to sort overexpressed TAU with similar efficiency than endogenous TAU, which makes these cells suitable for studying the key factors of TAU sorting.

TAU^{HA} lacking the C-terminus shows no axonal sorting in both neuronal model systems

We next tested the sorting efficiency of a truncated version of TAU. For this purpose, we transfected a truncated TAU^{HA} lacking the C-terminus (N-term-TAU^{HA}), and analyzed the sorting efficiency in SH-SY5Y-derived and mouse primary neurons (Fig. 4, Suppl.Fig. 2), as former studies suggested an important role of the N-terminus for axonal sorting [42]. However, our experiments showed no axonal enrichment of N-term-TAU^{HA} in SH-SY5Y-derived neurons ($AEF_{TAU_HA} = 0.97 \pm 0.03$; t-test for difference from 1.0: $p = 0.44$, n.s.) and even slight somatic enrichment in mouse primary neurons ($AEF_{TAU_HA} = 0.85 \pm 0.07$; t-test for difference from 1.0: $p = 0.03$, *) (Fig. 4A,C,D, Suppl.Fig. 2). Moreover, this truncated TAU^{HA} version tended to accumulate in the soma, indicated by the HA-positive puncta (Fig. 4A, Suppl.Fig. 2). These results strongly suggest that the N-terminal half of TAU is either not involved in the process of axonal sorting or at least not sufficient for its successful implementation.

No ANKG enrichment at the AIS region in SH-SY5Y-derived neurons despite efficient axonal TAU sorting

Finally, we evaluated the formation of the axon initial segment (AIS), essential for the maintenance of neuronal polarity, in SH-SY5Y-derived neurons (Fig. 5). The scaffold protein ANKG is a master organizer of the AIS architecture as it recruits AIS-located scaffold proteins, ion channels or cytoskeletal elements [35,37,38]. Therefore, we examined the accumulation of ANKG at the proximal axon as a measure of AIS formation (Fig. 5). We observed strong enrichment of ANKG at the first 50 µm of the proximal axon in div9 mouse primary neurons (Fig. 5C,D), which is in line with previous findings [73]. In contrast, ANKG was not enriched at the proximal axon of SH-SY5Y-derived neurons (Fig. 5A,B,E), independent of different fixation procedures (see methods for details) that were reported as expedient for AIS detection [74,75]. In other words, SH-SY5Y-derived neurons can efficiently sort endogenous TAU and overexpressed 0N3R-TAU^{HA} without visible ANKG accumulation at the proximal axon. This indicates that the process of axonal TAU sorting is independent of detectable ANKG enrichment at the AIS in these neurons.

Discussion

Mislocalization of the axonal TAU protein is a hallmark of Alzheimer's disease and related tauopathies. In this study, we first aimed to generate a neuronal cell model, derived from SH-SY5Y cells, as a suitable model for studying axonal TAU sorting. We then used SH-SY5Y-derived neurons and mouse primary neurons i) to evaluate the subcellular sorting of a truncated version of TAU ii) to test the previously reported AIS-dependence of efficient axonal TAU sorting.

First, we evaluated SH-SY5Y-derived neurons regarding their suitability for research on axonal TAU sorting mechanisms. Sequential treatment with RA/BDNF generated the highest number of neurons showing pronounced axon outgrowth, high expression levels of TAU and MAP2 and efficient axonal sorting of TAU, which was comparable to that of mouse primary neurons. This goes in line with previous studies, where the use of serum-free medium led to pure and stable SH-SY5Y-derived neuron cultures, when BDNF was administered [55,76,77]. Neuronal polarity and TAU sorting were less pronounced in SH-SY5Y-derived neurons produced with RA, TPA or TPA treatments. Based on these findings, we decided to conduct all further experiments with RA/BDNF-treated SH-SY5Y-derived neurons. An often-faced problem of primary murine cultures is the inefficient sorting of transfected TAU constructs [41,49,78]. This effect was also observed in our study, where sorting efficiency of 0N3R-TAU^{HA} was roughly 50 % less than for endogenous TAU in mouse primary neurons. Strikingly, in SH-SY5Y-derived neurons the axonal enrichment of this overexpressed construct reached comparable levels (~ 94 %) to endogenous TAU. One reason for that might be that SH-SY5Y-derived neurons tolerate the protein overexpression for at least nine days, while primary neurons largely died after more than three days of tdTomato or TAU^{HA} overexpression. The longer cultivation time may facilitate the axonal targeting of 0N3R-TAU^{HA}, as the plasmid DNA may become degraded after several days and the protein overload may decrease with increasing time and allow more efficient sorting of the transfected protein. Further reasons for the seen differences could be general sorting differences between mouse and human TAU, but this remains to be investigated. Mouse primary neurons possibly express a different set of isoforms that is more efficiently sorted than 0N3R-TAU. However, 0N3R-TAU is the predominant isoform in early developmental stages [3,79], which may include div9 neurons derived from E13.5 embryonic mice, and this isoform was sorted most efficiently in previous studies [40,78]. In brief, SH-SY5Y-derived neurons share properties of often-used neuronal models for TAU sorting as rodent primary neurons [39–42] or iPSC-derived neurons [43–47]. But these cells overcome several of their limitations, as they are human-derived, cultivatable at low cost and without the need to sacrifice animals, as a neuroblastoma cell line readily accessible for genetic engineering [67,68], and transfected TAU^{HA} is sorted similar to endogenous TAU, which is difficult to achieve in rodent primary cultures [41,49,78].

In the next step, we used SH-SY5Y-derived neurons to analyze whether HA-tagged TAU protein lacking the C-terminal half (N-term-TAU^{HA}) is still efficiently sorted. The axonal enrichment of N-term-TAU^{HA} was around 1.0 in SH-SY5Y-derived neurons and mouse primary neurons, i.e. resembling the subcellular distribution of the randomly distributed volume marker tdTomato. N-term-TAU^{HA} accumulates within the soma in

subcellular compartments, possibly lysosomes or stress granules, of transfected SH-SY5Y-derived and mouse primary neurons, maybe hinting at the increased accumulation tendency of N-term-TAU^{HA} or enhanced cellular degradation resulting from protein quality control mechanisms. In brief, N-term-TAU^{HA} is not enriched in the axonal compartment and shows somatic accumulation. These findings are interesting, since recent studies claimed a major role for the very N-terminal TAU domain [42] and the P-rich domain [41], both are present in N-term-TAU^{HA}, in axonal TAU sorting. Our results suggest that these domains are either not involved in TAU sorting in our neuronal models or at least not sufficient to maintain the intracellular sorting processes. As former studies suppose that MTs play a role for axonal TAU sorting [34,40], the missing C-terminus, which is critical for MT-binding of TAU [13,14], may be necessary for efficient sorting. However, recent findings question the role of the MT-binding repeat domains for TAU sorting [41]. More effort is required to shed light on the TAU-intrinsic properties that ensure efficient TAU sorting. SH-SY5Y-derived neurons are a valuable tool to conduct further and more comprehensive studies.

The formation of the AIS at the proximal part of the axon is critical for the development and maintenance of neuronal polarity, and for the polarized distribution of proteins [35,37]. There is strong evidence that the AIS and the integrity of its architecture play a major role in regulating the anterograde and retrograde trafficking of TAU [33,34,39,40]. Unravelling the mechanisms and involved components of selective TAU transit and retention at the AIS is critical to understand TAU sorting in general. Therefore, we finally evaluated the AIS formation in SH-SY5Y-derived neurons that show robust axonal enrichment of TAU. Interestingly, no accumulation of ANKG, a master organizer of the AIS architecture, was detectable within the putative AIS region or anywhere else along the axon of SH-SY5Y-derived neurons, in contrast to mouse primary neurons, where robust ANKG enrichment was observed at the proximal axon. It is interesting that the strong axonal sorting of endogenous and transfected TAU apparently does not require ANKG formation at the AIS, although it is responsible for the recruitment of major AIS structural components [35]. Thereby, our data suggest that neuronal outgrowth and efficient axonal targeting of TAU are independent of ANKG and the ANKG-mediated AIS assembly. The question arises, which other factors could be responsible for axonal TAU sorting in SH-SY5Y-derived neurons. The recruitment of the tripartite motif containing protein 46 (TRIM46) at the AIS – prior to ANKG accumulation – might be involved in axonal retention of TAU [73,80], and the end binding protein 3 (EB3) may play a role in anterograde TAU transit [47]. Interestingly, both proteins interact with the dense MT filaments within the AIS [47,80]. However, it is still unclear whether MTs or other components play a role in a potential TRIM46-mediated TAU retention, and whether EB3 or TRIM46 directly influence anterograde TAU transit.

Conclusion

In this study, we demonstrate that SH-SY5Y-derived neurons, generated with RA/BDNF treatment, are a suitable and powerful tool for investigating TAU sorting mechanisms. These neuronal cells show pronounced neuronal polarity, neuronal marker expression, efficient sorting of endogenous and, importantly, of transfected 0N3R-TAU^{HA}. Thereby, SH-SY5Y-derived neurons not only share properties of often-used neuronal models for TAU sorting, but also overcome several of their limitations. By using SH-SY5Y-derived neurons, we show that the N-terminal half of TAU is not

sufficient for successful axonal sorting, and that axonal TAU targeting is independent of ANKG recruitment to the AIS. Taken together, our data highlight that SH-SY5Y-derived neurons are a valuable tool for studying TAU sorting mechanisms.

Acknowledgments

We thank Prof. Dr. Rudolf Wiesner (Institute for Veg. Physiology II, University Hospital Cologne) for providing us the SH-SY5Y neuroblastoma cell line. Animals were obtained from the CMMC animal facility and the CECAD in vivo research facility (both Cologne, Germany). This work was funded by the Else-Kröner-Fresenius Stiftung, Cologne Fortune, and supported by a doctoral fellowship of the Studienstiftung des deutschen Volkes. The authors declare that they have no competing interests.

Author contributions

MB: study design, experimental conduct, data acquisition, analysis, and interpretation, manuscript drafting. SB: manuscript proofreading, assistance in methodology development. JK: experimental conduct, assistance in data acquisition and analysis. FL: assistance in experimental conduct (molecular biology). HZ: project funding, study design, data interpretation, manuscript drafting.

References

1. Binder, L. I., Frankfurter, A. & Rebhun, L. I. The distribution of tau in the mammalian central nervous central nervous. *J. Cell Biol.* (1985). doi:10.1083/jcb.101.4.1371

2. Kempf, M., Clement, A., Faissner, A., Lee, G. & Brandt, R. Tau binds to the distal axon early in development of polarity in a microtubule- and microfilament-dependent manner. *J. Neurosci.* (1996).

3. Goedert, M., Spillantini, M. G., Jakes, R., Rutherford, D. & Crowther, R. A. Multiple isoforms of human microtubule-associated protein tau: sequences and localization in neurofibrillary tangles of Alzheimer's disease. *Neuron* (1989). doi:10.1016/0896-6273(89)90210-9

4. Andreadis, A., Brown, W. M. & Kosik, K. S. Structure and Novel Exons of the Human τ Gene. *Biochemistry* (1992). doi:10.1021/bi00158a027

5. Weingarten, M. D., Lockwood, A. H., Hwo, S. Y. & Kirschner, M. W. A protein factor essential for microtubule assembly. *Proc. Natl. Acad. Sci. U. S. A.* (1975). doi:10.1073/pnas.72.5.1858

6. Cleveland, D. W., Hwo, S. Y. & Kirschner, M. W. Physical and chemical properties of purified tau factor and the role of tau in microtubule assembly. *J. Mol. Biol.* (1977). doi:10.1016/0022-2836(77)90214-5

7. Drechsel, D. N., Hyman, A. A., Cobb, M. H. & Kirschner, M. W. Modulation of the dynamic instability of tubulin assembly by the microtubule-associated protein tau. *Mol. Biol. Cell* (1992). doi:10.1091/mbc.3.10.1141

8. Drubin, D. G., Feinstein, S. C., Shooter, E. M. & Kirschner, M. W. Nerve growth factor-induced neurite outgrowth in PC12 cells involves the coordinate induction of microtubule assembly and assembly-promoting factors. *J. Cell Biol.* (1985). doi:10.1083/jcb.101.5.1799

9. Hirokawa, N., Shiomura, Y. & Okabe, S. Tau proteins: the molecular structure and mode of binding on microtubules. *J. Cell Biol.* (1988). doi:10.1083/jcb.107.4.1449

10. Caceres, A. & Kosik, K. S. Inhibition of neurite polarity by tau antisense oligonucleotides in primary cerebellar neurons. *Nature* (1990). doi:10.1038/343461a0

11. Esmaeli-Azad, B., McCarty, J. H. & Feinstein, S. C. Sense and antisense transfection analysis of tau function: Tau influences net microtubule assembly, neurite outgrowth and neuritic stability. *J. Cell Sci.* (1994).

12. Dixit, R., Ross, J. L., Goldman, Y. E. & Holzbaur, E. L. F. Differential regulation of dynein and kinesin motor proteins by tau. *Science (80-.).* (2008). doi:10.1126/science.1152993

13. Butner, K. A. & Kirschner, M. W. Tau protein binds to microtubules through a flexible array of distributed weak sites. *J. Cell Biol.* (1991). doi:10.1083/jcb.115.3.717

14. Goedert, M., Wischik, C. M., Crowther, R. A., Walker, J. E. & Klug, A. Cloning and sequencing of the cDNA encoding a core protein of the paired helical filament of Alzheimer disease: Identification as the microtubule-associated protein tau. *Proc. Natl. Acad. Sci. U. S. A.* (1988). doi:10.1073/pnas.85.11.4051

15. Chen, J., Kanai, Y., Cowan, N. J. & Hirokawa, N. Projection domains of MAP2 and tau determine spacings between microtubules in dendrites and axons. *Nature* (1992). doi:10.1038/360674a0

16. Brandt, R., Léger, J. & Lee, G. Interaction of tau with the neural plasma membrane mediated by tau's amino-terminal projection domain. *J. Cell Biol.* (1995). doi:10.1083/jcb.131.5.1327

17. Gauthier-Kemper, A. *et al.* The frontotemporal dementia mutation R406W blocks tau's interaction with the membrane in an annexin A2-dependent manner. *J. Cell Biol.* (2011). doi:10.1083/jcb.201007161

18. Brion, J. P., Passareiro, H., Nunez, J. & Flament-Durand, J. MISE EN EVIDENCE

IMMUNOLOGIQUE DE LA PROTEINE TAU AU NIVEAU DES LESIONS DE DEGENERESCENCE NEUROFIBRILLAIRE DE LA MALADIE D'ALZHEIMER. *Arch. Biol. (Liege).* (1985).

19. Wischik, C. M. *et al.* Isolation of a fragment of tau derived from the core of the paired helical filament of Alzheimer disease. *Proc. Natl. Acad. Sci. U. S. A.* (1988). doi:10.1073/pnas.85.12.4506

20. Braak, H. & Braak, E. Neuropathological stageing of Alzheimer-related changes. *Acta Neuropathologica* (1991). doi:10.1007/BF00308809

21. Selkoe, D. J. The Molecular of Alzheimer ' s Pathology Disease Review. *Neuron* (1991). doi:10.1016/0896-6273(91)90052-2

22. Arriagada, P. V., Growdon, J. H., Hedley-Whyte, E. T. & Hyman, B. T. Neurofibrillary tangles but not senile plaques parallel duration and severity of Alzheimer's disease. *Neurology* (1992).

23. Braak, H., Duyckaerts, C., Braak, E. & Piette, F. Neuropathological stageing of Alzheimer related changes correlates with psychometrically assessed intellectual status. *Neurobiol. Aging* (1992). doi:10.1016/0197-4580(92)90298-c

24. Ishihara, T. *et al.* Age-dependent emergence and progression of a tauopathy in transgenic mice overexpressing the shortest human tau isoform. *Neuron* (1999). doi:10.1016/S0896-6273(00)81127-7

25. Zhang, B. *et al.* Retarded axonal transport of R406W mutant tau in transgenic mice with a neurodegenerative tauopathy. *J. Neurosci.* (2004). doi:10.1523/JNEUROSCI.0797-04.2004

26. Roy, S., Zhang, B., Lee, V. M. Y. & Trojanowski, J. Q. Axonal transport defects: A common theme in neurodegenerative diseases. *Acta Neuropathologica* (2005). doi:10.1007/s00401-004-0952-x

27. Ittner, L. M. *et al.* Dendritic function of tau mediates amyloid-β toxicity in alzheimer's disease mouse models. *Cell* (2010). doi:10.1016/j.cell.2010.06.036

28. Lacroix, B. *et al.* Tubulin polyglutamylation stimulates spastin-mediated microtubule severing. *J. Cell Biol.* (2010). doi:10.1083/jcb.201001024

29. Zempel, H., Thies, E., Mandelkow, E. & Mandelkow, E.-M. A Oligomers Cause Localized Ca2+ Elevation, Missorting of Endogenous Tau into Dendrites, Tau Phosphorylation, and Destruction of Microtubules and Spines. *J. Neurosci.* (2010). doi:10.1523/jneurosci.2357-10.2010

30. Zempel, H. *et al.* Amyloid-β oligomers induce synaptic damage via Tau-dependent microtubule severing by TTLL6 and spastin. *EMBO J.* (2013). doi:10.1038/emboj.2013.207

31. Zempel, H. & Mandelkow, E. M. Tau missorting and spastin-induced microtubule disruption in neurodegeneration: Alzheimer Disease and Hereditary Spastic Paraplegia. *Molecular Neurodegeneration* (2015). doi:10.1186/s13024-015-0064-1

32. Ittner, A. & Ittner, L. M. Dendritic Tau in Alzheimer's Disease. *Neuron* (2018). doi:10.1016/j.neuron.2018.06.003

33. Zempel, H. & Mandelkow, E. Mechanisms of Axonal Sorting of Tau and Influence of the Axon Initial Segment on Tau Cell Polarity. in *Advances in Experimental Medicine and Biology* (2019). doi:10.1007/978-981-32-9358-8_6

34. Scholz, T. & Mandelkow, E. Transport and diffusion of Tau protein in neurons. *Cellular and Molecular Life Sciences* (2014). doi:10.1007/s00018-014-1610-7

35. Rasband, M. N. The axon initial segment and the maintenance of neuronal polarity. *Nature Reviews Neuroscience* (2010). doi:10.1038/nrn2852

36. Jones, S. L. & Svitkina, T. M. Axon Initial Segment Cytoskeleton: Architecture, Development, and Role in Neuron Polarity. *Neural Plasticity* (2016). doi:10.1155/2016/6808293

37. Leterrier, C. The Axon Initial Segment, 50 Years Later: A Nexus for Neuronal Organization and Function. *Curr. Top. Membr.* (2016). doi:10.1016/bs.ctm.2015.10.005

38. Leterrier, C. The axon initial segment: An updated viewpoint. *J. Neurosci.* (2018). doi:10.1523/JNEUROSCI.1922-17.2018

39. Li, X. *et al.* Novel diffusion barrier for axonal retention of Tau in neurons and its failure in neurodegeneration. *EMBO J.* (2011). doi:10.1038/emboj.2011.376

40. Zempel, H. *et al.* Axodendritic sorting and pathological missorting of Tau are isoform-specific and determined by axon initial segment architecture. *J. Biol. Chem.* (2017). doi:10.1074/jbc.M117.784702

41. Iwata, M., Watanabe, S., Yamane, A., Miyasaka, T. & Misonou, H. Regulatory mechanisms for the axonal localization of tau protein in neurons. *Mol. Biol. Cell* (2019). doi:10.1091/mbc.E19-03-0183

42. Gauthier-Kemper, A. *et al.* Annexins A2 and A6 interact with the extreme N terminus of tau and thereby contribute to tau's axonal localization. *J. Biol. Chem.* (2018). doi:10.1074/jbc.RA117.000490

43. Muratore, C. R. *et al.* The familial alzheimer's disease APPV717I mutation alters APP processing and Tau expression in iPSC-derived neurons. *Hum. Mol. Genet.* (2014). doi:10.1093/hmg/ddu064

44. Verheyen, A. *et al.* Using human iPSC-derived neurons to model TAU aggregation. *PLoS One* (2015). doi:10.1371/journal.pone.0146127

45. Silva, M. C. *et al.* Human iPSC-Derived Neuronal Model of Tau-A152T Frontotemporal Dementia Reveals Tau-Mediated Mechanisms of Neuronal Vulnerability. *Stem Cell Reports* (2016). doi:10.1016/j.stemcr.2016.08.001

46. Wang, C. *et al.* Scalable Production of iPSC-Derived Human Neurons to Identify Tau-Lowering Compounds by High-Content Screening. *Stem Cell Reports* (2017). doi:10.1016/j.stemcr.2017.08.019

47. Sohn, P. D. *et al.* Pathogenic Tau Impairs Axon Initial Segment Plasticity and Excitability Homeostasis. *Neuron* (2019). doi:10.1016/j.neuron.2019.08.008

48. Janke, C. *et al.* Phylogenetic diversity of the expression of the microtubule-associated protein tau: Implications for neurodegenerative disorders. *Mol. Brain Res.* (1999). doi:10.1016/S0169-328X(99)00079-0

49. Xia, D., Gutmann, J. M. & Gotz, J. Mobility and subcellular localization of endogenous, gene-edited Tau differs from that of over-expressed human wild-type and P301L mutant Tau. *Sci. Rep.* (2016). doi:10.1038/srep29074

50. Hu, B. Y. *et al.* Neural differentiation of human induced pluripotent stem cells follows developmental principles but with variable potency. *Proc. Natl. Acad. Sci. U. S. A.* (2010). doi:10.1073/pnas.0910012107

51. Gunhanlar, N. *et al.* A simplified protocol for differentiation of electrophysiologically mature neuronal networks from human induced pluripotent stem cells. *Mol. Psychiatry* (2017). doi:10.1038/mp.2017.56

52. Bell, S. *et al.* Differentiation of Human Induced Pluripotent Stem Cells (iPSCs) into an Effective Model of Forebrain Neural Progenitor Cells and Mature Neurons. *BIO-PROTOCOL* (2019). doi:10.21769/bioprotoc.3188

53. Biedler, J. L. & Schachner, M. Multiple Neurotransmitter Synthesis by Human Neuroblastoma Cell Lines and Clones. *Cancer Res.* (1978).

54. Kovalevich, J. & Langford, D. Considerations for the use of SH-SY5Y neuroblastoma cells in neurobiology. *Methods Mol. Biol.* (2013). doi:10.1007/978-1-62703-640-5_2

55. Encinas, M. *et al.* Sequential treatment of SH-SY5Y cells with retinoic acid and brain-derived neurotrophic factor gives rise to fully differentiated, neurotrophic factor-dependent, human neuron-like cells. *J. Neurochem.* (2000). doi:10.1046/j.1471-4159.2000.0750991.x

56. Cheung, Y. T. *et al.* Effects of all-trans-retinoic acid on human SH-SY5Y neuroblastoma as in

vitro model in neurotoxicity research. *Neurotoxicology* (2009). doi:10.1016/j.neuro.2008.11.001

57. Lopes, F. M. *et al.* Comparison between proliferative and neuron-like SH-SY5Y cells as an in vitro model for Parkinson disease studies. *Brain Res.* (2010). doi:10.1016/j.brainres.2010.03.102

58. Xie, H. R., Hu, L. Sen & Li, G. Y. SH-SY5Y human neuroblastoma cell line: In vitro cell model of dopaminergic neurons in Parkinson's disease. *Chinese Medical Journal* (2010). doi:10.3760/cma.j.issn.0366-6999.2010.08.021

59. Påhlman, S., Ruusala, A. I., Abrahamsson, L., Mattsson, M. E. K. & Esscher, T. Retinoic acid-induced differentiation of cultured human neuroblastoma cells: a comparison with phorbolester-induced differentiation. *Cell Differ.* (1984). doi:10.1016/0045-6039(84)90038-1

60. Gimenez-Cassina, A., Lim, F. & Diaz-Nido, J. Differentiation of a human neuroblastoma into neuron-like cells increases their susceptibility to transduction by herpesviral vectors. *J. Neurosci. Res.* (2006). doi:10.1002/jnr.20976

61. Agholme, L., Lindström, T., Kgedal, K., Marcusson, J. & Hallbeck, M. An in vitro model for neuroscience: Differentiation of SH-SY5Y cells into cells with morphological and biochemical characteristics of mature neurons. *J. Alzheimer's Dis.* (2010). doi:10.3233/JAD-2010-091363

62. Lee, M., McGeer, E. & McGeer, P. L. Activated human microglia stimulate neuroblastoma cells to upregulate production of beta amyloid protein and tau: Implications for Alzheimer's disease pathogenesis. *Neurobiol. Aging* (2015). doi:10.1016/j.neurobiolaging.2014.07.024

63. Smith, C. J., Anderton, B. H., Davis, D. R. & Gallo, J. M. Tau isoform expression and phosphorylation state during differentiation of cultured neuronal cells. *FEBS Lett.* (1995). doi:10.1016/0014-5793(95)01221-Y

64. Tanaka, T., Iqbal, K., Trenkner, E., Dong Jie Liu & Grundke-Iqbal, I. Abnormally phosphorylated tau in SY5Y human neuroblastoma cells. *FEBS Lett.* (1995). doi:10.1016/0014-5793(95)00061-D

65. Majd, S., Koblar, S. & Power, J. Compound C enhances tau phosphorylation at Serine396 via PI3K activation in an AMPK and rapamycin independent way in differentiated SH-SY5Y cells. *Neurosci. Lett.* (2018). doi:10.1016/j.neulet.2018.01.049

66. Majd, S., Majd, Z., Koblar, S. & Power, J. Beta estradiol and norepinephrine treatment of differentiated SH-SY5Y cells enhances tau phosphorylation at (Ser396) and (Ser262) via AMPK but not mTOR signaling pathway. *Mol. Cell. Neurosci.* (2018). doi:10.1016/j.mcn.2018.02.004

67. Bell, M. & Zempel, H. SH-SY5Y-derived Neurons: A Neuronal Model System for Investigating TAU Sorting Mechanisms and Neuronal Subtype-specific TAU Vulnerability. *Preprints.org* (2020). doi:10.20944/PREPRINTS202006.0203.V1

68. Sola, M. *et al.* Tau affects P53 function and cell fate during the DNA damage response. *Nat. Commun. Biol.* **3**, 245 (2020).

69. Påhlman, S., Odelstad, L., Larsson, E., Grotte, G. & Nilsson, K. Phenotypic changes of human neuroblastoma cells in culture induced by 12-O-tetradecanoyl-phorbol-13-acetate. *Int. J. Cancer* (1981). doi:10.1002/ijc.2910280509

70. Zempel, H. & Mandelkow, E. M. Tracking Tau in neurons: How to grow, fix, and stain primary neurons for the investigation of Tau in all developmental stages. in *Methods in Molecular Biology* (2017). doi:10.1007/978-1-4939-6598-4_20

71. Zempel, H., Luedtke, J. & Mandelkow, E. M. Tracking Tau in neurons: How to transfect and track exogenous tau into primary neurons. in *Methods in Molecular Biology* (2017). doi:10.1007/978-1-4939-6598-4_21

72. Tanapat, P. Neuronal Cell Markers. *Mater. Methods* (2013). doi:10.13070/mm.en.3.196

73. Kneynsberg, A., Vega, I. & Kanaan, N. M. TRIM46 KNOCKDOWN CAUSES NEURONAL TAU REDISTRIBUTION AND INCREASES AXOSOMATIC TAU DIFFUSION. *Alzheimer's Dement.*

(2019). doi:10.1016/j.jalz.2019.06.4852

74. Sohn, P. D. *et al.* Acetylated tau destabilizes the cytoskeleton in the axon initial segment and is mislocalized to the somatodendritic compartment. *Mol. Neurodegener.* **11**, (2016).

75. Di Re, J., Kayasandik, C., Botello-Lins, G., Labate, D. & Laezza, F. Imaging of the Axon Initial Segment. *Curr. Protoc. Neurosci.* (2019). doi:10.1002/cpns.78

76. Arcangeli, A. *et al.* Modulation of HERG current and herg gene expression during retinoic acid treatment of human neuroblastoma cells: Potentiating effects of BDNF. *J. Neurobiol.* (1999). doi:10.1002/(SICI)1097-4695(199908)40:2<214::AID-NEU7>3.0.CO;2-0

77. Shipley, M. M., Mangold, C. A. & Szpara, M. L. Differentiation of the SH-SY5Y human neuroblastoma cell line. *J. Vis. Exp.* (2016). doi:10.3791/53193

78. Bachmann, S., Bell, M., Klimek, J. & Zempel, H. Subcellular localization of TAU isoforms and their influence on microtubule dynamics. *bioRxiv* 2020.06.16.154757 (2020). doi:10.1101/2020.06.16.154757

79. Trabzuni, D. *et al.* MAPT expression and splicing is differentially regulated by brain region: Relation to genotype and implication for tauopathies. *Hum. Mol. Genet.* (2012). doi:10.1093/hmg/dds238

80. Van Beuningen, S. F. B. *et al.* TRIM46 Controls Neuronal Polarity and Axon Specification by Driving the Formation of Parallel Microtubule Arrays. *Neuron* (2015). doi:10.1016/j.neuron.2015.11.012

Figures

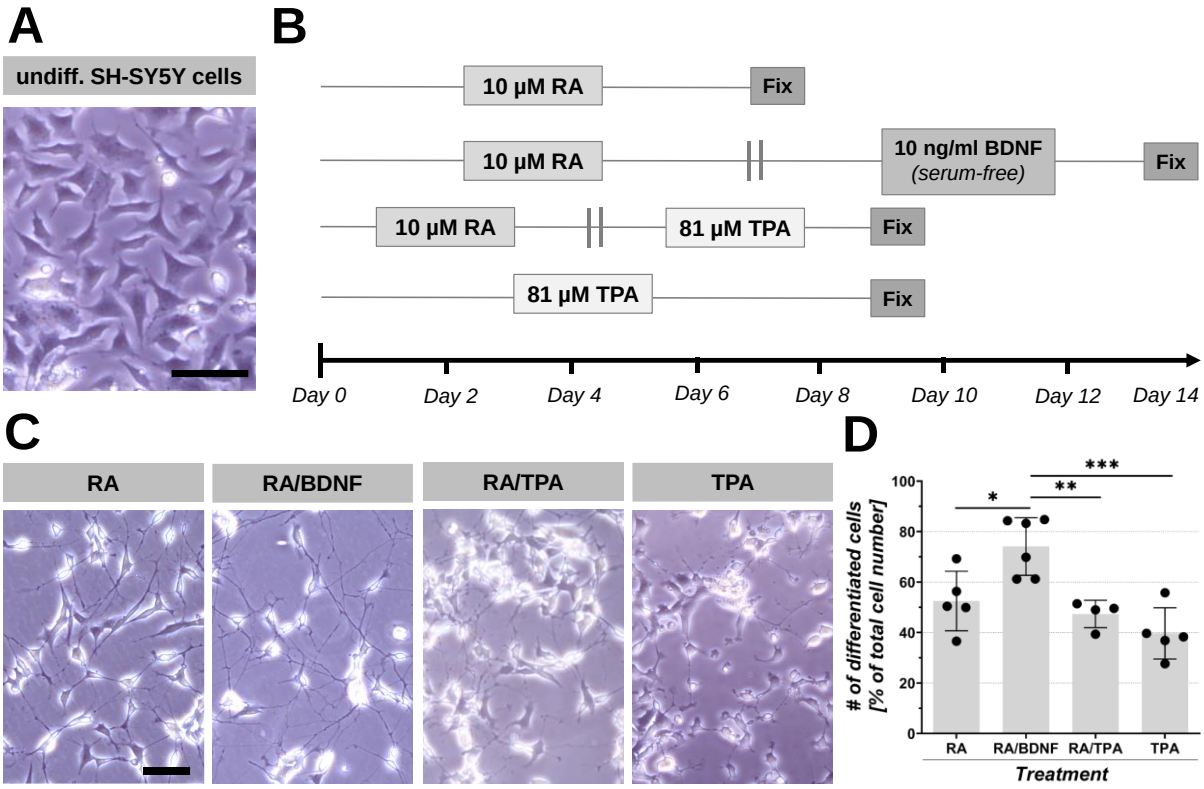

Figure 1: Generation of SH-SY5Y-derived neurons. Representative images of undifferentiated SH-SY5Y cells, timeline of differentiation procedures (see methods for details), and differentiated SH-SY5Y-derived neurons. **A:** Undifferentiated SH-SY5Y cells cultured in normal SHM-10 medium. Scale bar: 50 µm. **B:** Schematic time course of differentiation protocols. The bottom line indicates the day (d) of differentiation. **B.1:** RA was applied until d7 in SH-SY5Y cell culture medium with 10 % FBS (SHM-10). **B.2:** Sequential treatment with RA in SHM-10 until d7 and BDNF in serum-free SHM-0 medium until d14. **B.3:** Sequential treatment of RA in SHM-10 until d4 and TPA in SHM-10 until d9. **B.4:** Application of TPA in SHM-10 until d9. Black doubled lines indicate substance changes, grey box represents fixation of cells. **C:** SH-SY5Y-derived neurons after differentiation with RA, RA/BDNF, RA/TPA or TPA in culture. Note i) the neurite outgrowth of SH-SY5Y-derived neurons upon all treatments and ii) the different extent of co-cultured undifferentiated cells. Scale bar: 50 µm. **E:** Quantification of differentiation efficiency. Quantification was done for four to six independent experiments; 1000 ± 50 cells were counted per experiment per condition. Differentiated cells were determined with the differentiation criteria (see methods for details). Black dots represent independent experiments, grey bars indicate the arithmetic mean of all experiments, and error bars show SD. An ordinary one-way ANOVA and Tukey's correction for multiple comparisons were performed to determine significance levels between all four methods; * $p < 0.05$, ** $p < 0.01$, *** $p < 0.001$.

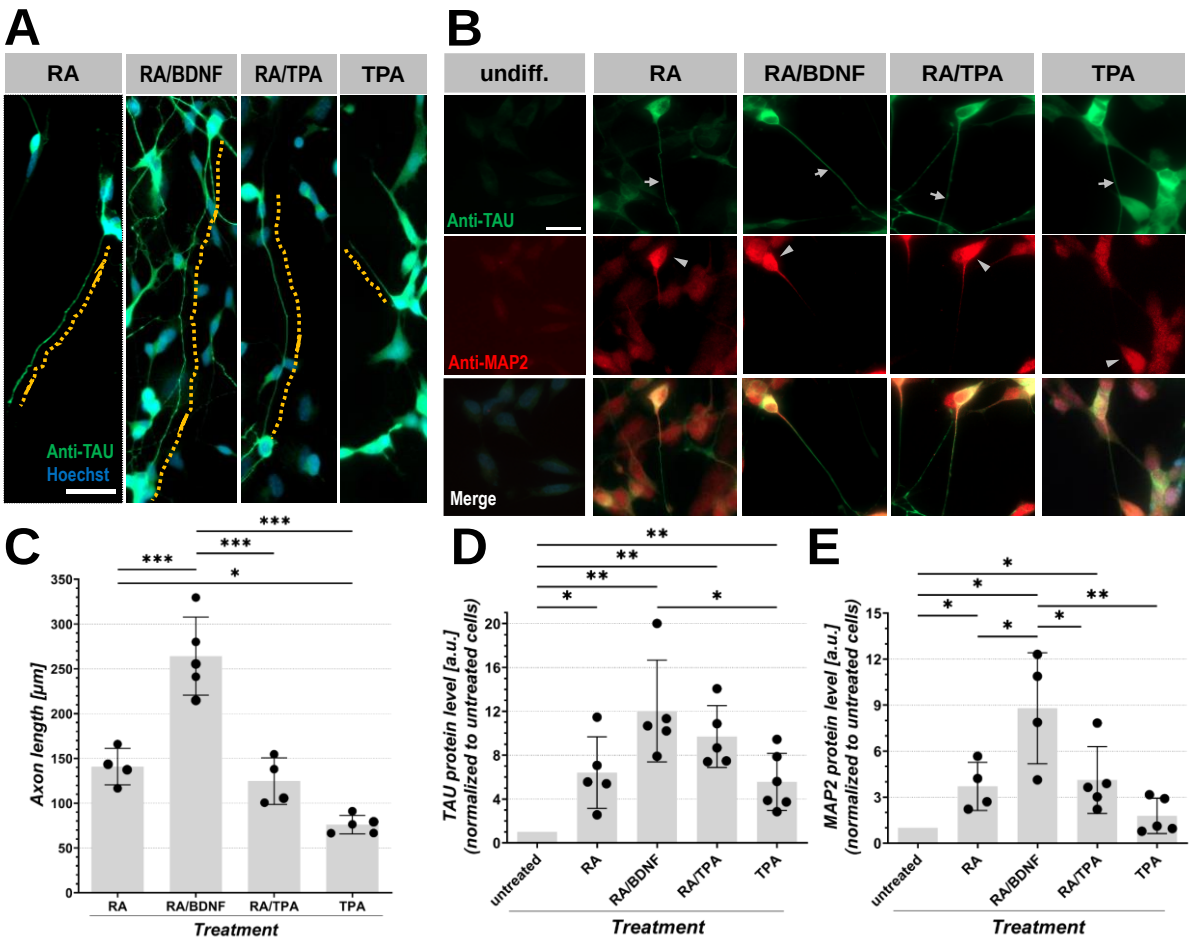

Fig. 2: Neuronal maturation of SH-SY5Y-derived neurons upon differentiation. A: Axonal outgrowth of SH-SY5Y-derived neurons after differentiation with RA, RA/BDNF, RA/TPA or TPA, immunostained with polyclonal anti-TAU (K9JA) antibody and NucBlue™ (nuclear staining). Dashed lines trace representative axons. Note the different extent of axonal elongation. Scale bar: 50 µm. **B:** Representative images of undifferentiated SH-SY5Y and SH-SY5Y-derived neurons immunostained with polyclonal anti-TAU (K9JA) and polyclonal anti-MAP2 antibodies. TAU (green) and MAP2 (red) are shown in single channels and merged. Note the weak signal of neuronal maturation markers TAU (green) and MAP2 (red) in undifferentiated cells (left panel) and the enhanced signals after differentiation as indicated. Scale bar: 20 µm; **C-E:** Analysis of neuronal maturation in SH-SY5Y-derived neurons, which were determined by nuclear and somatic shape, and neuritic outgrowth (see differentiation criteria (methods) for details). Quantification of axonal outgrowth (C) was done for four to five independent experiments; 30 – 35 cells were traced per experiment and per condition. Quantification for TAU (D) and MAP2 (E) protein levels was done for five to six (D) or four to five (E) independent experiments; 25 – 30 cells were measured per experiment and per condition. Black dots represent independent experiments, grey bars indicate the arithmetic mean of all experiments, and error bars show SD. An ordinary one-way ANOVA and Tukey's correction for multiple comparisons were performed to determine significance levels between all four treatments (C), and all four treatments and undifferentiated cells (D & E); * $p < 0.05$, ** $p < 0.01$, *** $p < 0.001$.

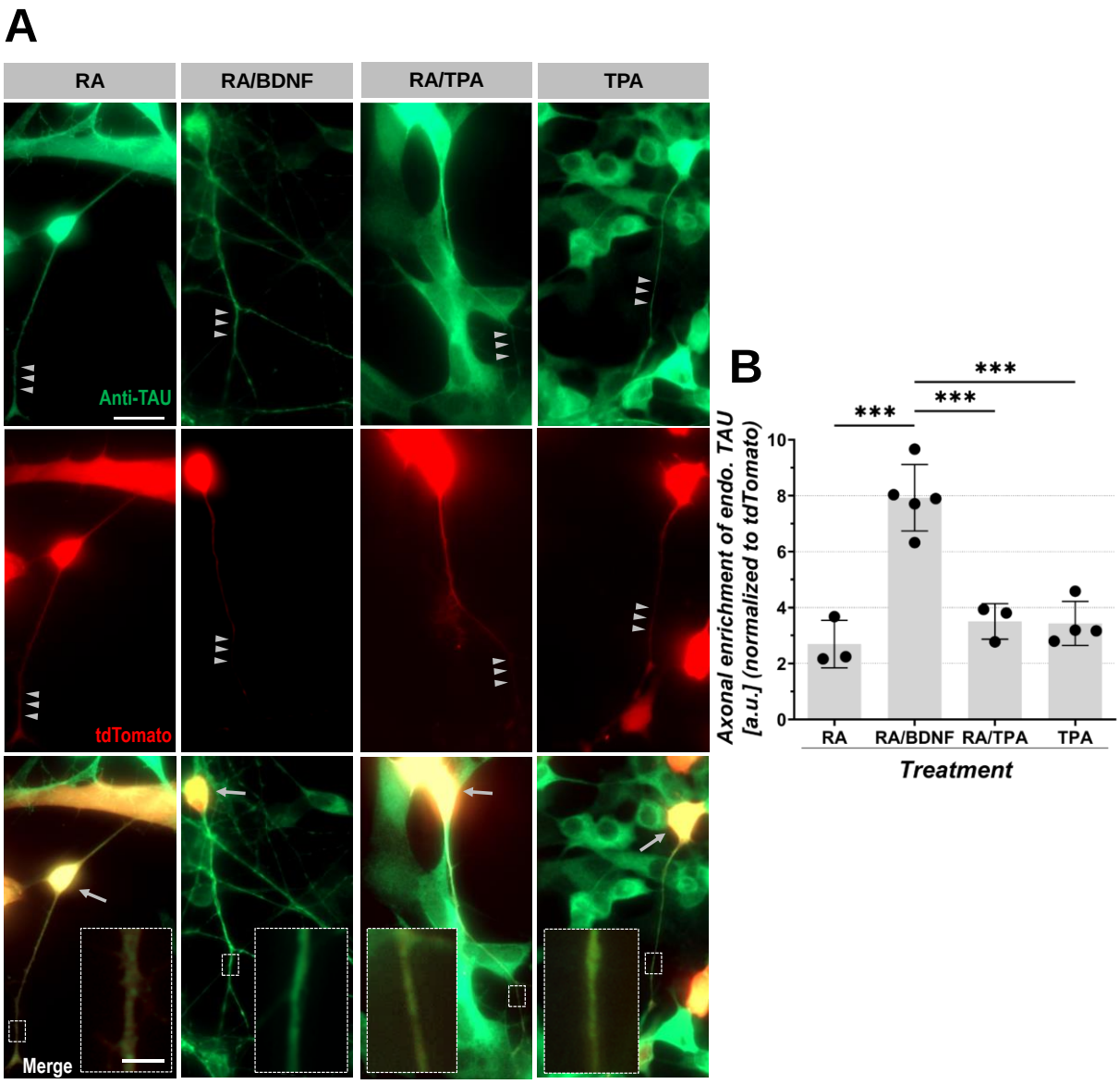

Figure 3: Axonal enrichment of endogenous TAU in SH-SY5Y-derived neurons. SH-SY5Y-derived neurons were transfected with tdTomato and immunostained with polyclonal anti-TAU (K9JA) antibody. **A:** Endogenous TAU (green) and transfected tdTomato as volume marker (red) are shown in single channels and merged. Note the strong axonal sorting of TAU compared to tdTomato (arrowheads) in SH-SY5Y-derived neurons after RA/BDNF treatment which leads to yellowish somatic staining (arrows) and mainly green axonal TAU staining in merged images. Axonal sections (small dashed boxes) are shown with higher magnification (large dashed boxes) in merged images. Scale bar: 20 µm, scale bar within dashed box: 3 µm. **B:** Quantification of the axonal enrichment of endogenous TAU ($AEF_{endoTAU}$), normalized to intracellular tdTomato distribution in neuronal cells (see methods for details). Quantification was done for three to five independent experiments; 20 – 30 cells were measured per experiment and per condition. Black dots represent independent experiments, grey bars indicate the arithmetic mean of all experiments, and error bars show SD. An ordinary one-way ANOVA and Tukey's correction for multiple comparisons were performed to determine significance levels between all conditions. * $p < 0.05$, ** $p < 0.01$, *** $p < 0.001$; * $p < 0.05$, ** $p < 0.01$, *** $p < 0.001$, n.s.: $p \geq 0.05$.

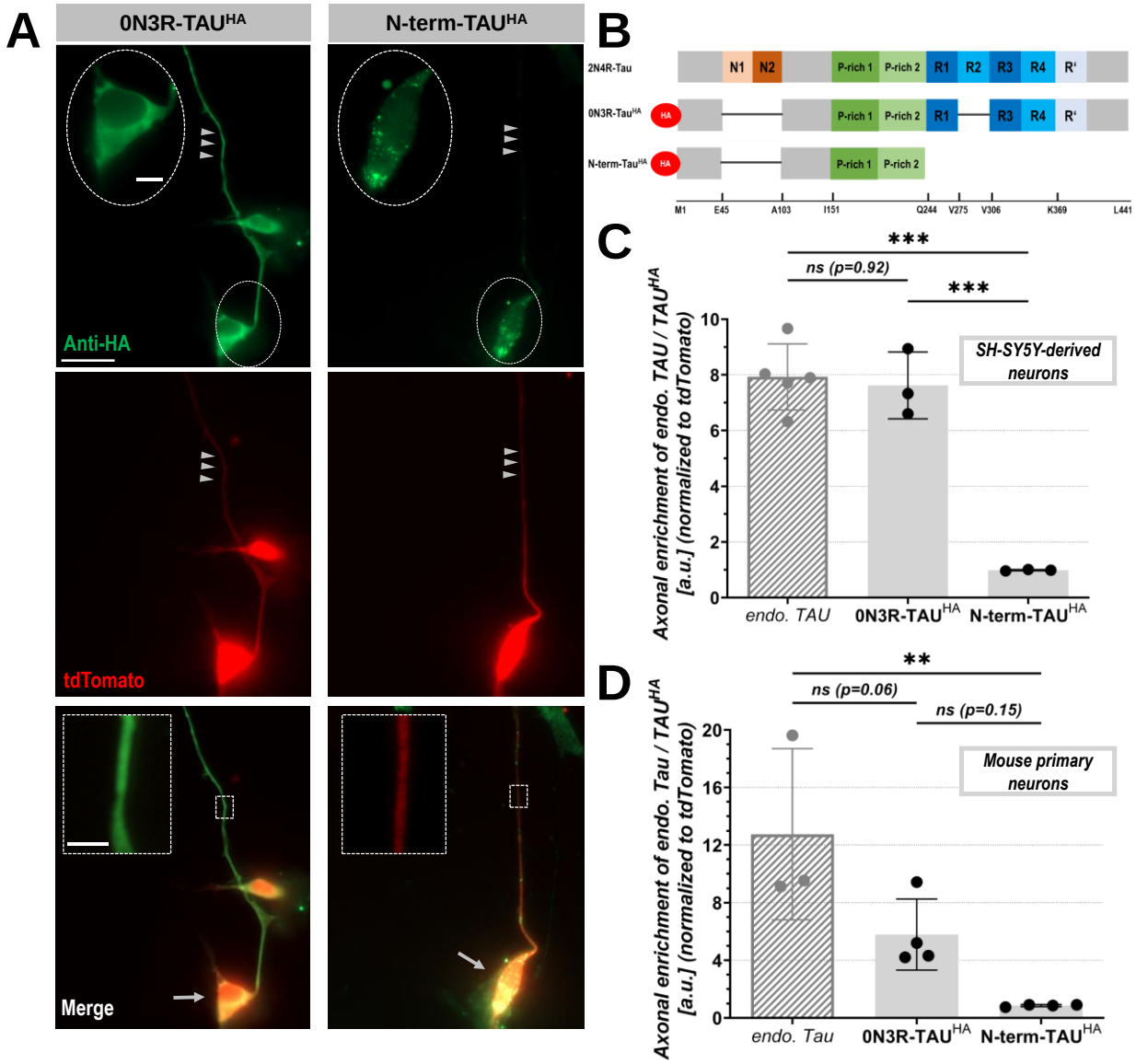

Figure 4: Axonal enrichment of transfected TAU^{HA} constructs in RA/BDNF-treated SH-SY5Y-derived and primary mouse neurons. A: Representative immunofluorescent images of SH-SY5Y-derived neurons transfected with tdTomato and either 0N3R-TAU^{HA} (left column) or N-term-TAU^{HA} (right column). TAU^{HA} constructs (green) and co-transfected tdTomato as volume marker (red) are shown in single channels and merged. Cells were transfected at d5 and fixed at d14 (see methods for details). Note the strong axonal sorting of TAU compared to tdTomato (arrowheads) in 0N3R-TAU^{HA} which leads to yellowish somatic staining (arrows) and mainly green axonal staining in merged images. Axons of cells with N-term-TAU^{HA} appear orange, indicating weak axonal sorting of N-term-TAU^{HA}. Axonal sections (small dashed boxes) are shown with higher magnification (large dashed boxes). HA-positive puncta (small dashed circle, magnified in large dashed circle) appear in N-term-TAU^{HA} transfected cells but not in cells expressing 0N3R-TAU^{HA}. Scale bar: 20 µm, scale bar within dashed circle: 5 µm, scale bar within dashed box: 3 µm. **B:** Domain structure of full-length 2N4R-TAU compared to the used TAU constructs. 0N3R-TAU^{HA} contains the amino acids M1 – E45, A103 – V275 and V306 – L441. N-term-TAU^{HA} contains the amino acids M1 – E45 and A103 – V244. Missing parts are represented by black lines. Both constructs were N-terminally fused to an HA tag (red circle). The bottom line indicates selected amino acid positions. N1/N2: N-terminal inserts, P-rich domain: Proline-rich domain, R1 – R4: C-terminal repeat domains. R': Pseudo-repeat domain. **C & D:** Quantification of axonal enrichment of TAU^{HA} constructs (AEF_{TAU_HA}) in SH-SY5Y-derived neurons (C) and mouse primary neurons (D), normalized to intracellular tdTomato distribution. Axonal enrichment of endogenous TAU/Tau (striped bars,

see Fig. 3A) is included for comparison. Quantification was done for three to four independent experiments with up to three technical replicates (C, D) or one experiment with four technical replicates (D, N-term-TAU^{HA}). For each replicate, 15 – 20 cells were measured. For representative images of mouse primary neurons: see Fig. S2. Black dots represent independent experiments, grey bars indicate the arithmetic mean of all experiments, and error bars show SD. An ordinary one-way ANOVA and Tukey's correction for multiple comparisons were performed to determine significance levels between endogenous TAU/Tau and the TAU^{HA} constructs. * $p < 0.05$, ** $p < 0.01$, *** $p < 0.001$, n.s.: $p \geq 0.05$.

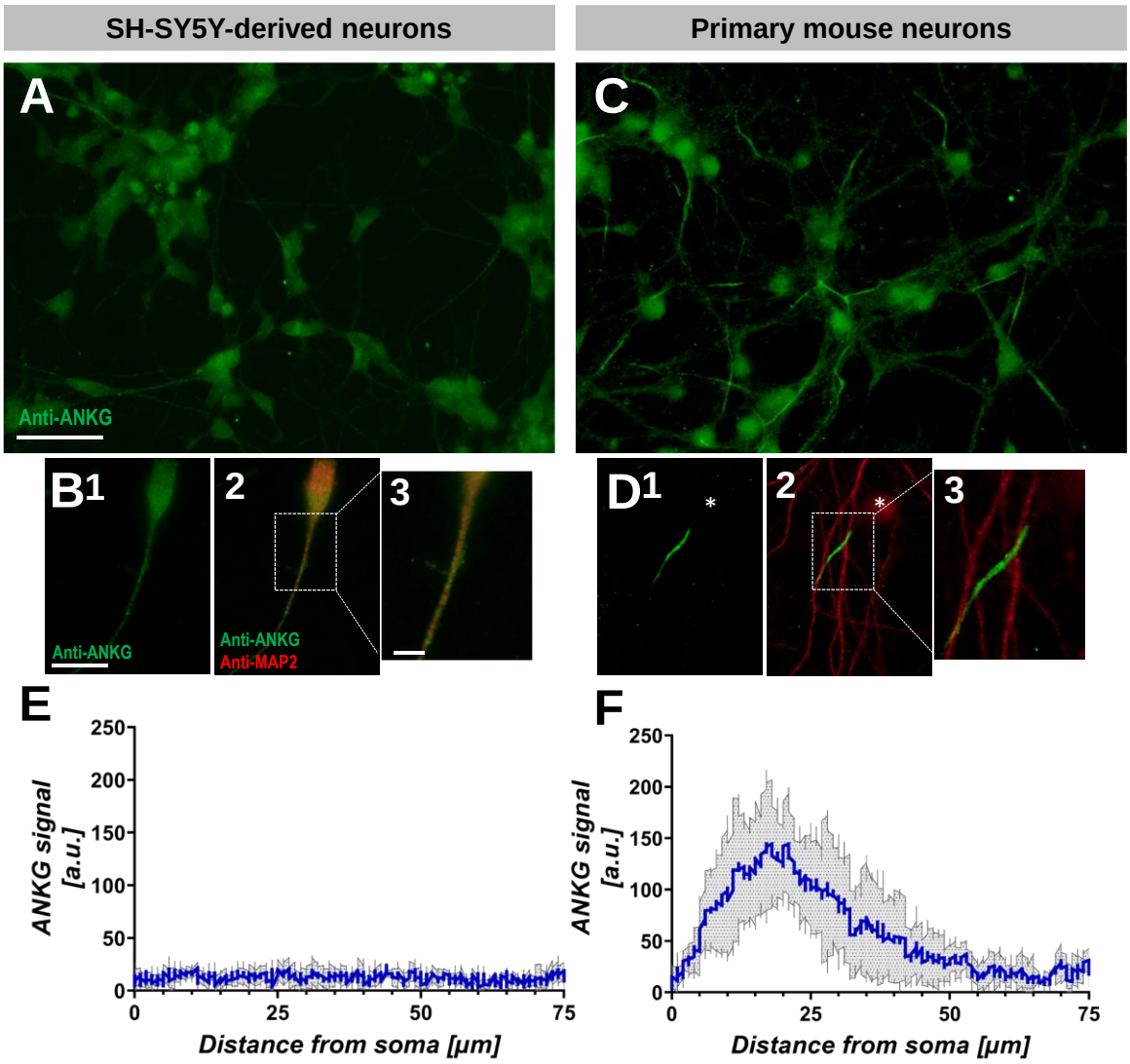

Figure 5: Formation of the AIS in SH-SY5Y-derived and primary mouse neurons. A-D: Representative images of ANKG expression in SH-SY5Y-derived neurons (A & B) and mouse primary neurons (C & D), immunostained with monoclonal anti-ANKG and polyclonal anti-MAP2 antibodies. **A & C:** Overview of immunostained neuronal cultures. Scale bar: 50 µm. **B & D:** Representative immunostained SH-SY5Y-derived (B) and primary mouse neurons (D). Proximal axon sections (small dashed boxes, B.2 & D.2) are shown with higher magnification (B.3 & D.3). Note the clearly defined enrichment of ANKG at the proximal axon of div9 mouse primary neurons, which is not visible in SH-SY5Y-derived neurons. Asterisks indicate cell somata. Scale bar (B.1): 20 µm, scale bar (B.3): 5 µm. **E & F:** Plot profiles of ANKG fluorescent signal in SH-SY5Y-derived (E) and primary mouse neurons (F) at the proximal axon. The blue lines indicate the arithmetic mean of three independent experiments; 20 – 25 cells were traced and measured per experiment and per condition (see methods for details). The grey area shows SD.